Korean J. Chem. Eng., **20**(4), 601-608 (2003)

Two Phase Visualization by Electrical Impedance Tomography with Prior Information

Min Chan Kim†, Kyoung Youn Kim* and Sin Kim**

Department of Chemical Engineering, *Department of Electrical and Electronic Engineering,
**Department of Nuclear and Energy Engineering, Cheju National University, Cheju 690-756, Korea
(*Received 10 December 2001 • accepted 6 February 2003*)

Abstract−Numerical and experimental work was conducted to develop a visualization technique for the phase distribution in a two-phase flow field with known internal structures by electrical impedance tomography technique, which reconstructs the resistivity distribution with the electrical responses that are determined by corresponding excitations. The finite element method is employed to solve the electrical field induced by the currents through electrodes placed along the boundary and a modified Newton-Raphson iterative method is used to determine the search step minimizing the error between the calculated and the measured voltages at the electrodes. The locations and resisitivities of the known structures are considered as prior information. To mitigate the ill-posedness of inverse problem and to incorporate prior information, the modified Tikhonov regularization technique is employed. Also, with an apparatus developed for impedance imaging this study attempts to reconstruct the images of the simulated bubble distributions and the reconstructed images imply the potential possibility of the electrical impedance tomography for the two-phase flow visualization.

Key words: Image Reconstruction, Electrical Impedance Tomography, Modified Newton-Raphson Method, Internal Structure, Prior Information, Tikhonov Regularization

INTRODUCTION

Two-phase flow can occur under normal and accidental conditions in various processes such as heat exchanger, oil or natural gas pumping system and nuclear power plant. Because the heterogeneous phase distribution affects the safety, control, operation and optimization of the process, it is important to know the characteristics of two-phase flow field. Various non-destructive techniques such as laser Doppler velocimetry (LDV) and particle image velocimetry (PIV) have been developed to visualize the two-phase flow without disturbing the flow field. Recently, the electrical impedance tomography (EIT) technique originating from medical engineering is employed to investigate two-phase flow phenomena, because it is relatively inexpensive and has good time resolution [Webster, 1990; Jones et al., 1993; Cho et al., 1999, 2001]. The data acquisition time and the spatial resolution of state-of-art EIT system reach a few ms and 5%, respectively [Ovacik and Jones, 1998].

In EIT technology, different current patterns are applied to the flow field through the electrodes attached on the boundary and the corresponding voltages are measured. Based on the current-voltage relation, the internal resistivity distribution, that is, the phase distribution, is reconstructed. The numerical algorithm used to convert the boundary measurement data to the internal resistivity distribution consists of iteratively solving the forward problem and updating the conductivity distribution as determined by the formulation of inverse problem. The forward problem of EIT calculates the boundary voltages by using assumed resistivity distribution, and the inverse problem reconstructs the impedance distribution by using boundary voltage measurements.

Quite often in real situations there are known fixed internal structures and/or resistivities inside the object. These internal structures can be, for example, an impeller drive shaft or a mixing paddle in process vessels and fuel assemblies in nuclear reactors. The internal structures inside the object may result in difficulties in the image reconstruction in EIT especially in the case where the high resistive region is near the conductive internal structure [Williams et al., 1996; Heikkinen et al., 2001a]. The so-called masking effect in the reconstructed image may be significant for the high-contrast case. There are two ways to get around these difficulties; one is to use the internal structures as additional electrodes [Lyon and Oakley, 1993; Williams et al., 1996; Heikkinen et al., 2001a] and the other is to include the information on the internal structures (location, resistivity) as prior information in the inverse procedure [Heikkinen et al., 2001b].

The purpose of the present work is to develop an EIT system for the cases in which the fixed internal structure and/or its resistivity are known *a priori*. To achieve the purpose, an additional constraint for the known internal structure and/or its resistivity is incorporated into the object functional to account for prior information. The inverse problem is treated as the optimization problem and the unknown variable (resistivity) is estimated with the aid of the Newton-Raphson method in a minimum mean square error sense. In order to deal with the well-known ill-posedness of the EIT inverse problem, the modified Tikhonov regularization technique is also introduced. We carried out phantom experiments to illustrate the reconstruction performance with real measurement data, and to investigate the effects of priori information on the spatial resolution.

FORMULATION OF THE PROBLEMS AND FORWARD SOLVER

When electrical currents $I_l (l=1, 2, \cdots, L)$ are injected into the object $\Omega \in \Re^2$ through the electrodes $e_l (l=1, 2, \cdots, L)$ attached on

†To whom correspondence should be addressed.
E-mail: mckim@cheju.ac.kr

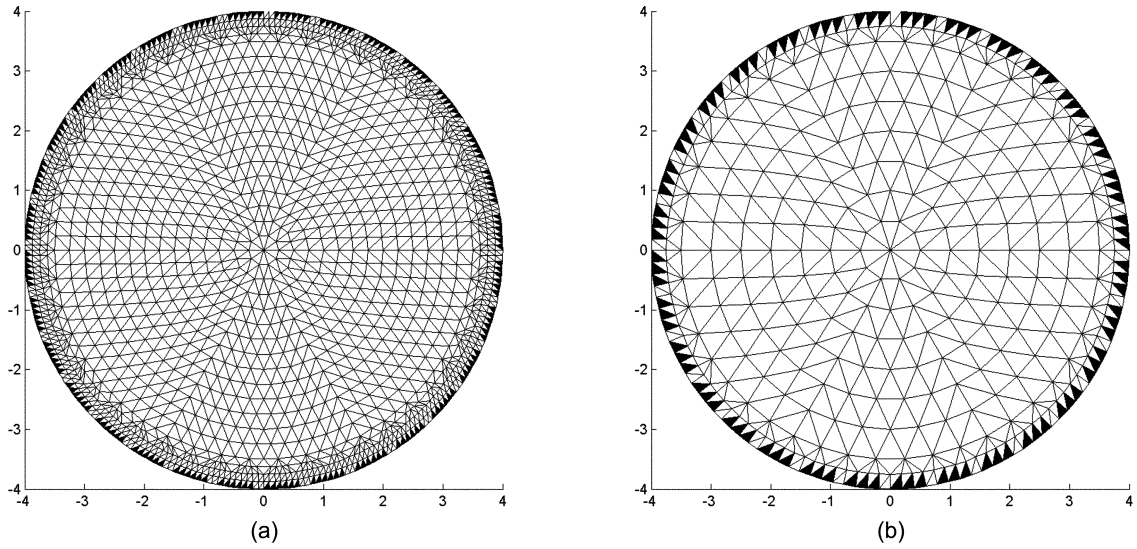

Fig. 1. FEM meshes for (a) forward solver and (b) inverse solver. Locations of the electrodes are marked with darkened elements.

the boundary $\partial\Omega$ and the resistivity distribution is known over the Ω, the corresponding electrical potential u(x) on Ω can be determined uniquely from the partial differential equation, which can be derived from Maxwell's equations:

$$\nabla\cdot\left(\frac{1}{\rho}\nabla u\right)=0 \qquad \text{in } \Omega \tag{1}$$

with the following boundary conditions based on the complete electrode model (CEM) [Vauhkonen, 1997]:

$$u+\frac{z_l}{\rho}\frac{\partial u}{\partial \nu}=U_l \qquad x\in e_l,\ l=1, 2, \cdots, L \tag{2}$$

$$\int_{e_l}\frac{1}{\rho}\frac{\partial u}{\partial \nu}dS=I_l \qquad x\in e_l,\ l=1, 2, \cdots, L \tag{3}$$

$$\frac{1}{\rho}\frac{\partial u}{\partial \nu}=0 \qquad x\in \partial\Omega\setminus\cup_{l=1}^{L}e_l \tag{4}$$

where z_l is the effective contact impedance between the lth electrode and the electrolyte, U_l is the potential on the lth electrode, ν stands for the outward unit normal, and L is the number of electrodes. Various forms of the boundary conditions have been proposed for the forward model, among them we choose the CEM which takes into account the discrete electrodes, the effects of the contact impedance, and the shunting effect of the electrodes.

In addition, the following two constraints for the injected currents and the measured voltages are needed to ensure the existence and uniqueness of the solution:

$$\sum_{l=1}^{L}I_l=0, \tag{5}$$

$$\sum_{l=1}^{L}U_l=0. \tag{6}$$

The computation of the potential u(x) on Ω and the voltages U_l on the electrodes for the given resistivity distribution ρ(x) and boundary conditions is called the forward problem. In general, the forward problem cannot be solved analytically; thus we have to resort to the numerical method. There are various numerical methods such as the finite difference method (FDM), boundary element method (BEM), and finite element method (FEM). In this study, we used the FEM to obtain numerical solution. In FEM, the object area is discretized into sufficiently small elements having a node at each corner and it is assumed that the resistivity distribution is constant within each element. The maximum amount of independent information is L(L−1), therefore in order to avoid making the problem overdetermined, the following relation should be satisfied.

$$N\geq\frac{L(L-1)}{2} \tag{7}$$

where N is the number of elements whose resistivities are unknown and L is the number of electrodes. In the present study, N=776 and L=32 are used for the inverse problem and N=3104 and L=32 for the forward problem as shown in Fig. 1.

Let M be the number of nodes in the finite element mesh, which is shown in Fig. 1. The potential distribution within the object is approximated as

$$u\approx u^h(x)=\sum_{i=1}^{M}\alpha_i\phi_i(x) \tag{8}$$

and the potential on the electrodes represented as

$$U^h=\sum_{j=1}^{L-1}\beta_j n_j \tag{9}$$

where the function ϕ_i is the two-dimensional first order basis function and the bases for the measurements are $n_1=(1, -1, 0, \Lambda, 0)^T$, $n_2=(1, 0, -1, 0, \Lambda, 0)^T$, $\Lambda\in\Re^{L\times 1}$, *etc.* That is, the potentials U_λ^h on the electrodes are obtained as

$$\begin{aligned}U_1^h&=\sum_{l=1}^{L-1}\beta_l\\ U_2^h&=-\beta_1\\ U_3^h&=-\beta_2\\ &\vdots\\ U_L^h&=-\beta_{L-1}\end{aligned} \tag{10}$$

which can be written in matrix form as

$$U^h = \mathbf{N}\beta. \tag{11}$$

This choice for n_j's ensures that the condition (6) is fulfilled. The following system of linear equations is obtained from the finite element formulation

$$\mathbf{A}b = I \tag{12}$$

where

$$b = \begin{pmatrix} \alpha \\ \beta \end{pmatrix} \quad \text{and} \quad I = \begin{pmatrix} 0 \\ \hat{I} \end{pmatrix} \tag{13}$$

and $\alpha=(\alpha_1, \alpha_2, \Lambda, \alpha_M)^T$, $\beta=(\beta_1, \beta_2, \Lambda, \beta_{L-1})^T$, $0 \in R^{M\times 1}$ and $\hat{I}=(I_1-I_2, I_1-I_3, \Lambda, I_1-I_L)^T$. The stiffness matrix A is of the form

$$\mathbf{A} = \begin{pmatrix} \mathbf{B} & \mathbf{CN} \\ (\mathbf{CN})^T & \mathbf{N}^T\mathbf{DN} \end{pmatrix} \tag{14}$$

where $\mathbf{N} \in \Re^{L\times(L-1)}$ is a sparse matrix having n_j's as column such that

$$\mathbf{N} = (n_1, n_2, \cdots, n_{L-1}) = \begin{pmatrix} 1 & 1 & \Lambda & 1 \\ -1 & 0 & \Lambda & 0 \\ 0 & -1 & \Lambda & 0 \\ \cdots & \cdots & \vdots & \cdots \\ 0 & 0 & \Lambda & -1 \end{pmatrix}. \tag{15}$$

The elements of the other matrices in matrix **A** are [Vauhkonen, 1997]

$$B(i,j) = \int_\Omega \frac{1}{\rho}\nabla\phi_i\nabla\phi_j dxdy + \sum_{\lambda=1}^{L}\frac{1}{z_\lambda}\int_{e_\lambda}\phi_i\phi_j dS, \quad i, j=1, 2, \Lambda, \cdots \tag{16}$$

$$C(i,j) = -\frac{1}{z_j}\int_{e_j}\phi_i dS, \quad i=1, 2, \cdots, M, j=1, 2, \cdots, L \tag{17}$$

$$D(i,j) = \begin{cases} 0 & i \neq j \\ \dfrac{|e_i|}{z_j} & i = j \end{cases} \quad i, j=1, 2, \cdots, L \tag{18}$$

where $|e_i|$ is the length of the electrode i.

In this study all the computations have been carried out in two-dimensional (2-D) case, corresponding to the cross-sections of the domain (see Fig. 2). If the rod shown in the figure is a good conductor having high conductivity, the electrical potential within the rod will be uniform. In 2-D finite element computations this type of a situation can be simulated by forcing the potentials of all nodes inside the rod region into the same value. This can be accomplished by making the following modification to the previous FEM formulations.

Let $W \subset \Omega$ be the subdomain including all the known structure. Define

$$\alpha = \mathbf{G}\gamma \tag{19}$$

where $\mathbf{G} \in \Re^{M\times(M-p+1)}$ and $\gamma=(\gamma_1, \gamma_2, \Lambda, \gamma_{M-p}, \gamma_w)^T \in \Re^{(M-p+1)\times 1}$. Also, p is the number of nodes in the subdomain $W \subset \Omega$ and γ_w is the value of the potential in W. The matrix **G** is a sparse matrix that maps

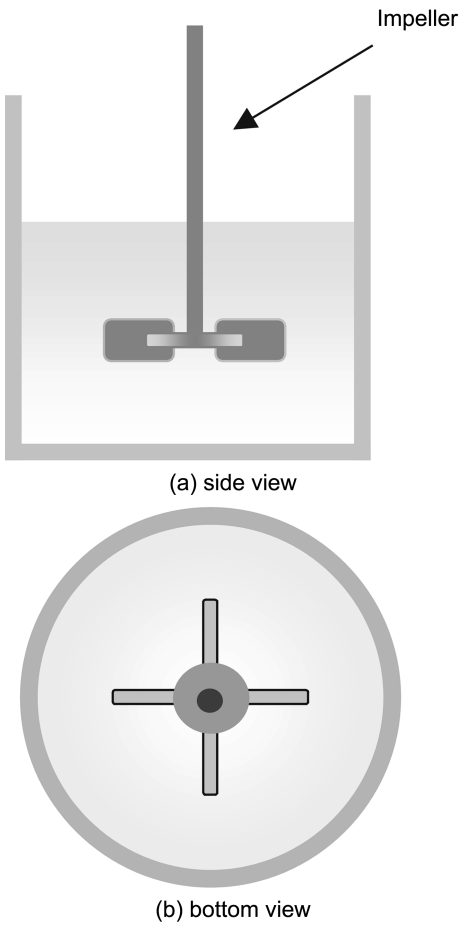

Fig. 2. Real situation.

the potential value γ_w to the potential of the corresponding nodes, namely the corresponding elements of α. After substituting the formula (18) into the matrix Eq. (11) we obtain

$$\tilde{\mathbf{A}}\tilde{b} = \tilde{I} \tag{20}$$

where

$$\tilde{\mathbf{A}} = \begin{pmatrix} \mathbf{G}^T\mathbf{BG} & \mathbf{G}^T\mathbf{CN} \\ (\mathbf{CN})^T\mathbf{G} & \mathbf{N}^T\mathbf{DN} \end{pmatrix} \tag{21}$$

and

$$\tilde{b} = \begin{pmatrix} \gamma \\ \beta \end{pmatrix} \quad \text{and} \quad \tilde{I} = \begin{pmatrix} \mathbf{G}^T 0 \\ \hat{I} \end{pmatrix}. \tag{22}$$

INVERSE SOLVER BASED ON THE NEWTON-RAPHSON METHOD

1. Newton-Raphson Method

The inverse problem of EIT maps the boundary voltages from experiments to resistivity image. The objective function may be chosen to minimize the error in the least square sense,

$$\Phi(\rho) = \frac{1}{2}[\mathbf{V}-\mathbf{U}(\rho)]^T[\mathbf{V}-\mathbf{U}(\rho)] \tag{23}$$

where $\mathbf{V}$ is the vector of measured voltage and $\mathbf{U}(\rho)$ is the calculated boundary voltage vector that must be matched to $\mathbf{V}$.

To find ρ which minimizes the above object function, its derivarivative is set to zero as:

$$\Phi'(\rho) = -[\mathbf{U}']^T[\mathbf{V}-\mathbf{U}] = 0 \tag{24}$$

where $[U']_{ij}=\partial U_i/\partial \rho_j$ is the Jacobian matrix. The solution of the above Eq. (24) uses the Newton-Raphson linearization about a resistivity vector ρ^k at k-th iteration as

$$\Phi'(\rho^{k+1}) = \Phi'(\rho^k) + \Phi''(\rho^k)(\rho^{k+1}-\rho^k) = 0. \tag{25}$$

The term Φ'' is called the Hessian matrix, expressed as

$$\Phi'' = [\mathbf{U}']^T\mathbf{U}' - [\mathbf{U}'']^T\{\mathbf{I}\otimes[\mathbf{V}-\mathbf{U}]\}. \tag{26}$$

where $\otimes$ is the Kronecker matrix product. Since $\mathbf{U}''$ is difficult to calculate and relatively small, the second term in the above Eq. (26) is usually omitted. Therefore the Hessian matrix is modified as

$$\Phi'' = [\mathbf{U}']^T\mathbf{U}' = \mathbf{J}^T\mathbf{J} = \mathbf{H}. \tag{27}$$

Thus, the iterative equation for updating the resistivity vector based on the above regularized object function is expressed as

$$\rho^{k+1} = \rho^k + \mathbf{H}^{-1}\{J^T(\mathbf{V}-\mathbf{U}(\rho^k))\} \tag{28}$$

where $\mathbf{J}$ and $\mathbf{H}$ are the Jacobian and the Hessian matrix, respectively.

2. Tikhonov Regularization

The Hessian matrix is known to be ill-conditioned, which then degrades the performance of the image reconstruction algorithm. To mitigate this problem, the objective function that should be minimized is regularized as:

$$\Phi(\rho) = [\mathbf{V}-\mathbf{U}(\rho)]^T[\mathbf{V}-\mathbf{U}(\rho)] + \lambda[\mathbf{R}(\rho-\rho^*)]^T[\mathbf{R}(\rho-\rho^*)] \tag{29}$$

where R is the regularization matrix, λ is the regularization parameter and ρ^* is the assumed resistivity vector. Consequently, the iterative equation to update the resistivity vector based on the above regularized object function is derived as

$$\rho^{k+1} = \rho^k + (\mathbf{J}^T\mathbf{J} + \lambda\mathbf{R}^T\mathbf{R})^{-1}\{\mathbf{J}^T(\mathbf{U}(\rho)-\mathbf{V}) - \lambda\mathbf{R}^T\mathbf{R}(\rho^k-\rho^*)\}. \tag{30}$$

According to the choice of R and ρ^*, one can have various regularizations like the first order difference (FOD) [Vauhkonen, 1997], the Levenberg-Marquardt (LM) regularization [Hua et al., 1988; Yorkey et al., 1987], the implicitly scaled Levenberg-Marquardt (isLM) regularization [Cheney et al., 1991] and so on. It is known that if the resistivity distribution can be assumed to be continuous FOD is a good choice and LM and isLM are suitable for the inverse problems whose iterative solutions are bounded but fluctuating [Webster, 1990]. These three regularization methods were tested numerically in the application of EIT to the visualization of two-phase flow [Kim et al., 2001]. The results indicated that isLM and FOD could reconstruct electrical resistance images very well even for measurement data contaminated by 2% errors and show good performance for high resistivity contrast system up to 1 : 1000. Hence, this study employs isLM, where $\mathbf{R}^T\mathbf{R}$ is modeled as a diagonal matrix whose diagonal components are those of $\mathbf{J}^T\mathbf{J}$, and $\rho^*=\rho^k$.

If the resistivity distribution can be assumed to be continuous, FOD regularization matrix $\mathbf{R}$ is chosen to be $|\mathbf{R}\rho| \approx |\nabla\rho|$. In this case, the gradient of the resistivity of the e-th element can be approximated in terms of the differences between the resistivity of e-th element and those of the nearest neighboring elements that share the face. If we discretize the problem domain into triangular elements the e-th row of the regularization matrix is given as

$$\mathbf{R}_e = [\Lambda \quad -1 \quad \Lambda \quad 3(\text{e-th}) \quad \Lambda \quad -1 \quad \Lambda \quad -1 \quad \Lambda] \tag{31}$$

A large regularization parameter forces the resistivity distribution to be constant. If $\lambda=0$, of course, the regularization method turns into the Newton-Raphson method.

3. Incorporating Known Information

Sometimes in real situations there are some known internal structures in the interior of the object. The known location and resistivity of the structure can be taken into account as prior information in the cost functional as

$$\Phi(\rho) = [\mathbf{V}-\mathbf{U}(\rho)]^T[\mathbf{V}-\mathbf{U}(\rho)] + \lambda[\mathbf{R}(\rho-\rho^*)]^T[\mathbf{R}(\rho-\rho^*)] + \chi[\mathbf{L}(\rho-\rho_*)]^T[\mathbf{L}(\rho-\rho_*)] \tag{32}$$

where the sparse matrix $\mathbf{L}$ is constructed to pick out the elements corresponding to the known structure. If we know the location and resistivities of q elements inside the object, $\rho_* \in \Re^{M\times 1}$ is constructed such that it contains the resistivity of q elements corresponding to the known structure and zeros of (M−q) elements, and the dimension of the extraction matrix is $L \in \Re^{q\times M}$. The j-th row of the extraction matrix, L_j is constructed such that it contains zeros for (M−1) elements and only one 1 at the j-th column if the j-th element in the struccture is known. In addition, χ is another weighting factor representing the confidence on the assumed resistivity of the internal structure. The value of χ can be chosen to be large if the resistivities of the internal structures are known accurately. If we know the location of the internal structure but not the resistivity, the value of χ is set to zero. Finally, the iterative equation to update the impedance vector based on the above object function is derived as

$$\rho^{k+1} = \rho^k + (\mathbf{J}^T\mathbf{J} + \lambda\,\mathrm{diag}(\mathbf{J}^T\mathbf{J}) + \chi\mathbf{L}^T\mathbf{L})^{-1}\{\mathbf{J}^T(\mathbf{U}(\rho)-\mathbf{V}) - \lambda\,\mathrm{diag}(\mathbf{J}^T\mathbf{J})(\rho^k-\rho^*) - \chi\mathbf{L}^T[\mathbf{L}(\rho^k-\rho_*)]\}. \tag{33}$$

IMAGE RECONSTRUCTION BASED ON PHANTOM EXPERIMENTS

Because of ill-posed characteristics of the EIT inverse problem, a practical test is important for evaluating the performance of the EIT system. We performed several phantom experiments and reconstructed images based on the experimental data to evaluate the performance of the proposed reconstruction algorithm and hardware setups.

1. Experiments

A cylindrical phantom with diameter 8 cm and height 33 cm is used. Thirty-two stainless steel electrodes are mounted on the inner surface of phantom and cover approximately 76% of the circumference. In order to obtain two-dimensional images, the electrodes are positioned at same height. The phantom was filled up with 0.15% saline solution having resistivity of 330 Ωcm. One cylindrical stainless steel rod with diameter of 1cm is located at the center of phantom. The location and the resistivity of stainless steel rod are assumed to be known, *a priori*. The cylindrical plastic targets with diameter of 1 cm, whose impedance is practically infinite, are placed in the phantom to simulate vapor phase.

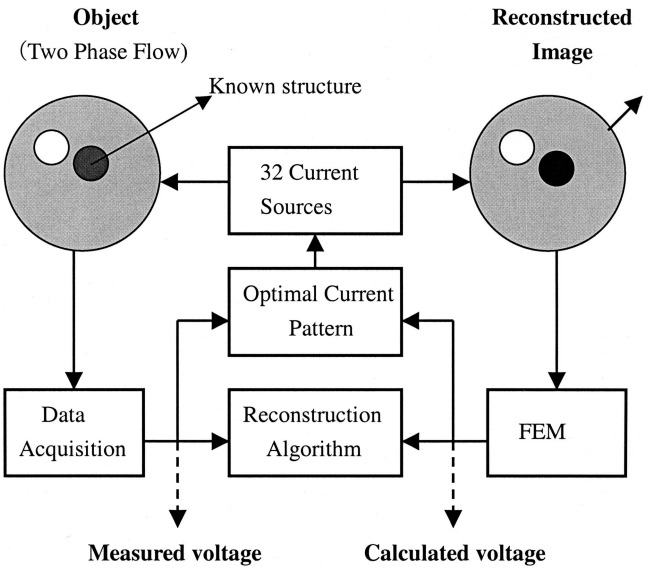

Fig. 3. Schematic diagram of EIT system.

The EIT system is described schematically in Fig. 3. The current generated by current generation circuit in the form of

$$I_l^m = \begin{cases} \cos(m\zeta_l) & l=1,2,\cdots,32, m=1,2,\cdots,16 \\ \sin(m\zeta_l) & l=1,2,\cdots,32, m=1,2,\cdots,15 \end{cases} \quad (34)$$

where $\zeta_l=2\pi l/32$, is injected into the 32 electrodes simultaneously, and the resulting voltages are measured. Total number of current patterns used in the experiments is 31. It is known that the above trigonometric current pattern gives best distinguishability and is the most versatile method of data collection [Webster, 1990]. The frequency of the current is 50 kHz. It is estimated that the errors involved in the generation of injected currents and in the measurement of boundary voltages for homogeneous medium are maintained less than 1%. The data acquisition time of our EIT system is a few ms, so tens of images can be obtained within 1s. Therefore, it is expected that bubble motion can be tracked with our EIT system. The obtained voltage distribution and the reconstructed image for the homogeneous saline water system are given in Fig. 4. As

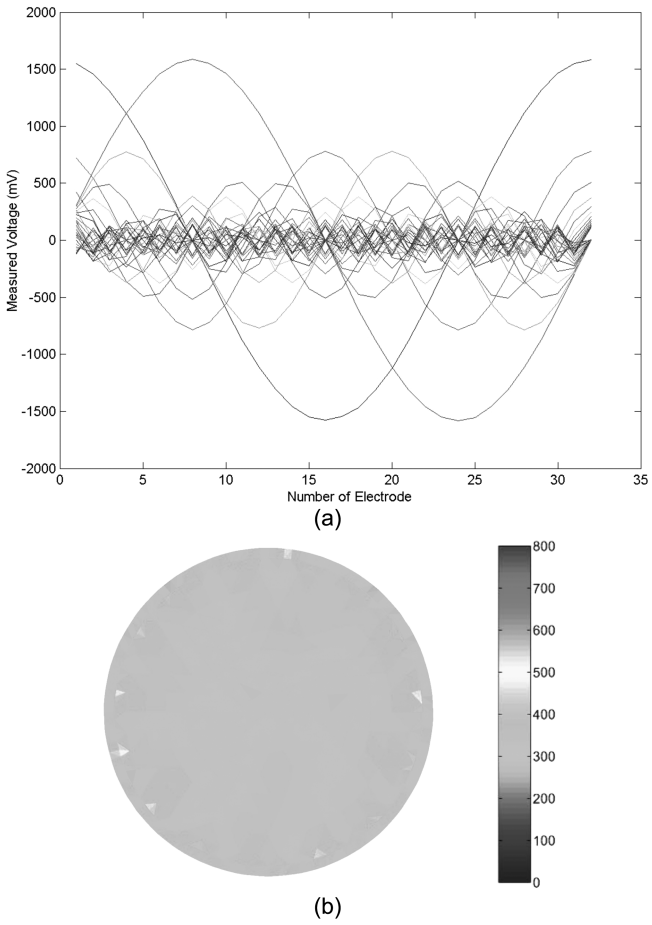

Fig. 4. Experimental result for homogeneous system. (a) measured voltage distribution and (b) reconstructed image. The regularization parameter is λ=0.5.

shown in this figure our EIT system and image reconstruction algorithm have reasonably good performance.

The proper initial guess is important, sometimes crucial, for the convergence of the inverse problem. If prior information on the object to be imaged is available one could attain a good convergence characteristic. Since, unlike medical EIT problems, the phase dis-

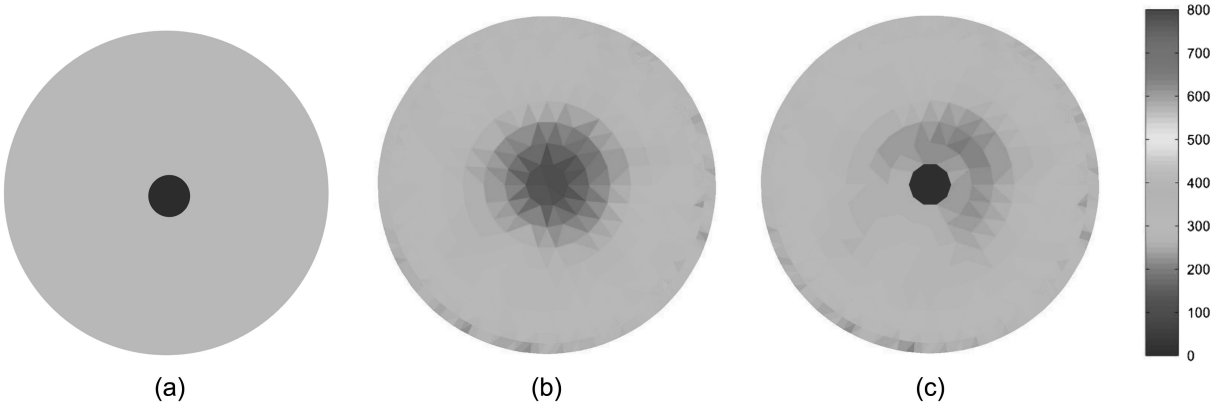

Fig. 5. Reconstructed image of no target system. (a) original image, (b) reconstructed image without prior information, and (c) reconstructed image with prior information. The regularization parameters are λ=0.5 and χ=2.

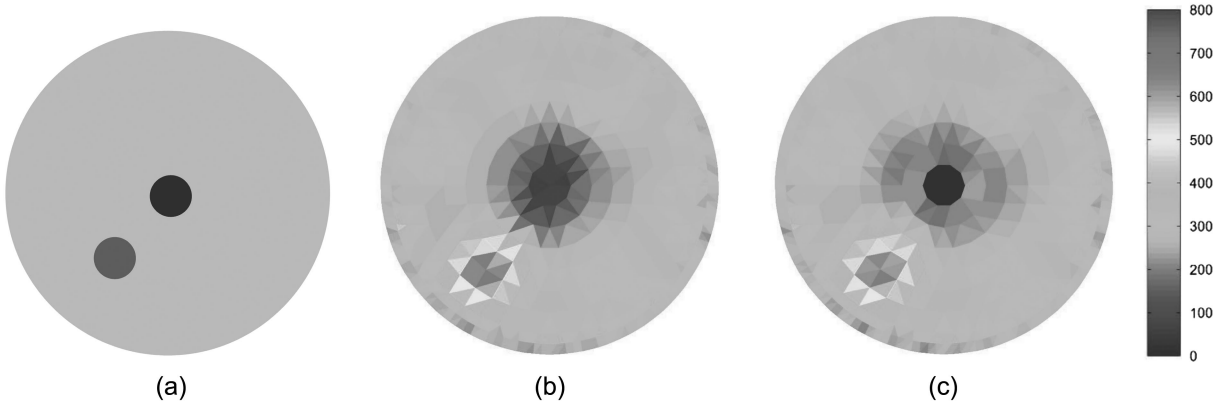

Fig. 6. Reconstructed image of one target system. (a) original image, (b) reconstructed image without prior information, and (c) reconstructed image with prior information. The regularization parameters are λ=0.5 and χ=2.

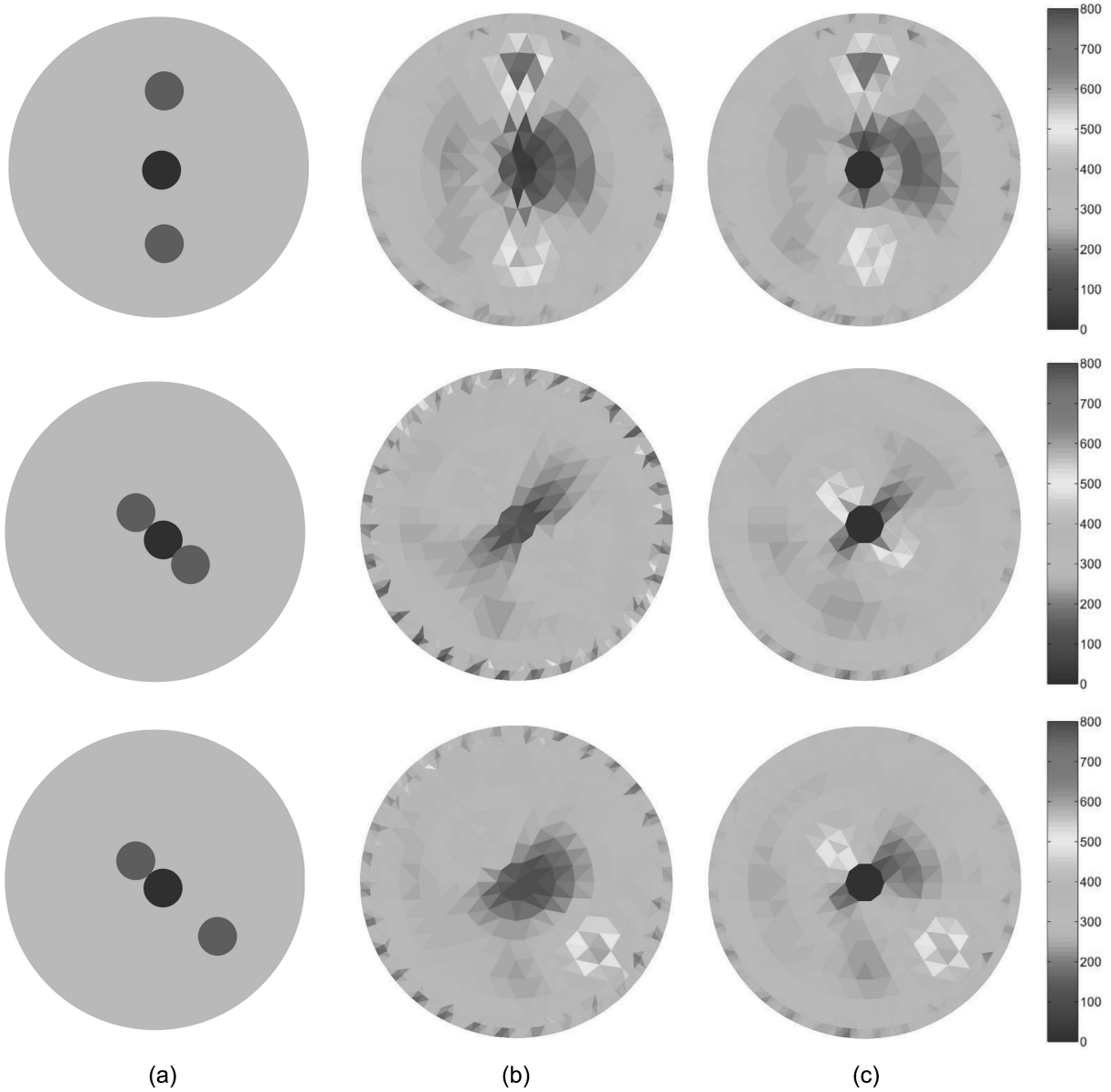

Fig. 7. Reconstructed image of two target system. (a) original images, (b) reconstructed images without prior information, and (c) reconstructed images with prior information. The regularization parameters are λ=0.5 and χ=2.

tribution in a two-phase flow is quite arbitrary, little information is known *a priori*. Hence, this study attempts to estimate a constant resistivity value representing the two-phase flow field considered instead of seeking a proper initial distribution. If one were to assume a linear relation between the boundary voltage and the internal resistivity, the boundary voltage is decomposed as

$$\frac{U_1(\rho)}{\rho} \approx \frac{U_1(\rho_r)}{\rho_r} \tag{35}$$

where ρ_r is an arbitrarily chosen constant resistivity. In the least square sense, a constant ρ_0 minimizing the following functional

$$\Phi_0 = \left[\mathbf{V} - \frac{\rho_0}{\rho_r}\mathbf{U}(\rho_r)\right]^T \left[\mathbf{V} - \frac{\rho_0}{\rho_r}\mathbf{U}(\rho_r)\right] \tag{36}$$

will be a good choice as an initial distribution.

The contact impedance that is caused by the imperfect contact between an electrode and an object is inevitable in reality. A problem with the contact impedance is that a relation between currents at electrodes and voltages across the object is not given for arbitrary real situations. Hence, before applying the EIT procedure to the real imaging problem, one needs to estimate the contact impedance, which will be considered in the reconstruction algorithm.

Invoking the contact impedance, the boundary voltage should be a function of the contact impedance as well as the interior resistivity distribution, U=U(ρ, z). Assume that the contact impedance remains unchanged during each experiment; one can fix the dependency of the resistivity distribution ρ by considering a homogeneous medium with a single phase. Namely, before each phantom experiment, in order to determine the contact impedance, one measures boundary voltages without inserting objects simulating bubbles. The contact impedance z that minimizes the following functional

$$\Phi_z = [\mathbf{V} - \mathbf{U}(\rho_s, z)]^T [\mathbf{V} - \mathbf{U}(\rho_s, z)] \tag{37}$$

is estimated in the sense of least square along with the aid of Eq. (2). In this, $\mathbf{V}$ is the homogeneous boundary voltage vector measured without dispersed phase, and ρ_s is the resistivity of the continuous phase, in the present experiment's saline solution. The contact impedance estimated in homogeneous situation is used for the image reconstruction of the distribution of the dispersed phase.

2. Reconstructed Images

Fig. 5 shows the effect of the prior information on the reconstructed image for no target system, i.e., water-conductor two phase system. For one target system, i.e., water-conductor-insulator three phase system, Fig. 6 describes the effect of the prior information. As shown in these figures, we can get clearer images with prior information than without. The effect of the prior information on the quality of the reconstructed image for this case is quite favorable. Especially, the effect of prior information is dramatically increased as the target approaches the rod located at the center of phantom, as shown in Fig. 7. As the target is near the rod, the predicted images without prior information become worse; however, the reconstructed image with prior information is not significantly affected by the relative position between the rod and the targets, as given in the second and third cases of Fig. 7. It should be noted that the predicted resistivities of the targets or the resistivity contrasts between two phases are not identical to each other. Nevertheless, from the reconstructed images with prior information one can identify the location of the bubble clearly and also estimate the size to a certain extent.

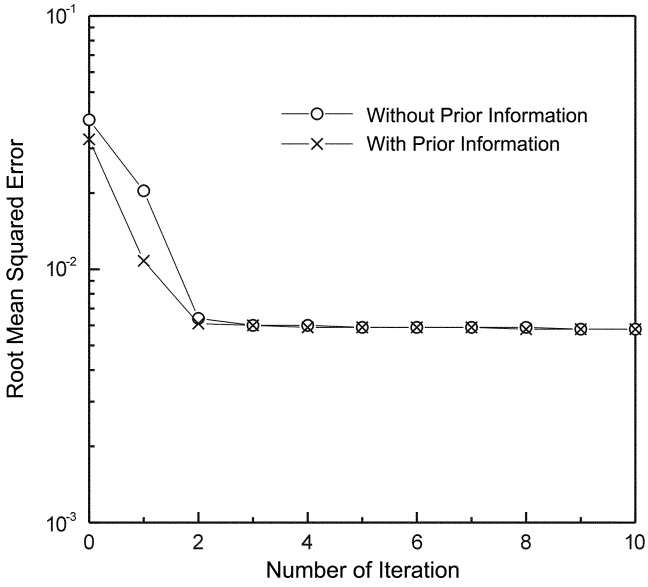

Fig. 8. Root mean squared error for the one target system (Fig. 6).

There are several methods for choosing optimal regularization parameters. However, different criteria will yield results of different optimality [Vauhkonen, 1997]. In this study, since the true distributions in experiments were known, the regularization parameters were chosen to show the best reconstruction image. These regularization parameters are set to λ=0.5 and χ=2 to treat the experimental error and prior information, respectively. If $\chi \geq 2$, the quality of reconstructed images and reconstruction time is not affected by χ.

The root mean square error (RMSE) defined as

$$\varepsilon = \sqrt{\frac{(\mathbf{U}-\mathbf{V})^T(\mathbf{U}-\mathbf{V})}{\mathbf{V}^T\mathbf{V}}} \tag{38}$$

for the one target system is given in Fig. 8. As shown in this figure, the RMSE decreases exponentially for the first two iteration, and shows nearly constant values after the third iteration. Even though the RMSE does not decrease after a few iterations, the quality of reconstructed image is continuously improved, so we set the maximum iteration number to 10.

CONCLUSIONS

Quite often in real situations, there are partially known fixed internal structures and/or resistivities inside the object. We have proposed an EIT reconstruction algorithm for the case in which a fixed internal structure and/or its resistivity are known and carried out phantom experiments to evaluate the performance of the EIT algorithm and to validate the EIT measurement system we have developed. We formulated the EIT inverse problem based on the Newton-Raphson method and incorporated additional information for the known internal structure and/or its resistivity into the object function which should be minimized. In addition, the modified Tikhonov regularization technique was employed to take into account the known internal structure. The quality of the reconstructed im-

ages based on the phantom experiments also says that the developed EIT system is able to generate the designed current signal and to measure the resulting voltages within the error range that can be coped with by the present EIT algorithm. Even there are some mismatches between the original images and the reconstructed images, from the reconstructed images with prior information one can identify the location of the bubble clearly and also estimate the size to a certain extent.

ACKNOWLEDGMENT

This work was supported by the Nuclear Academic Research Program of the Ministry of Science and Technology (MOST), Korea.

NOMENCLATURE

A : stiffness matrix used in Eq. (12)
B : matrix whose elements are given in Eq. (16)
b : force vector
C : matrix whose elements are given in Eq. (17)
D : matrix whose elements are given in Eq. (18)
G : mapping matrix
H : Hessian matrix
I : force vector used in Eq. (12)
I_l : injected electrical current through the *l*th electrode [A]
J : Jacobian matrix
N : matrix whose elements are given Eq. (15)
R : regularization matrix [-]
U : calculated boundary voltage matrix [V]
u : potential [V]
U_l : potential on the *l*th electrode [V]
V : measured voltage matrix [V]
z_l : effective contact impedance [Ωm^2]

Greek Letters

α : approximated potential vector used in Eq. (8) [V]
β : vector used in calculating the potentials at the electrodes
γ : potential vector mapped by matrix **G**
ε : root-mean squared error
λ : regularization parameter
ν : outward unit normal vector [m]
ρ : resisitivity [Ωm]
Φ : objective function [V^2]
ϕ : two-dimensional first order basis function [-]
χ : regularization parameter [-]

REFERENCES

Cheney, M., Isaacson, D., Nowell, J. C., Simske, S. and Globe, J., "NOSER; An Algorithm for Solving the Inverse Conductivity Problem," *Int. J. Imaging Systems Tech.*, **2**, 66 (1991).

Cho, K. H., Kim, S. and Lee, Y. J., "A Fast EIT Image Reconstruction Method for the Two-Phase Flow Visualization Method," *Int. Comm. Heat Mass Transfer*, **26**, 637 (1999).

Cho, K. H., Kim, S. and Lee, Y. J., "Impedance Imaging of Two-Phase Flow Field with Mesh Grouping Algorithm," *Nucl. Eng. Des.*, **204**, 57 (2001).

Heikkinen, L. M., Vauhkonen, M., Savolainen, T., Leinonen, K. and Kaipio, J. P., "Electrical Process Tomography with Known Internal Structures and Resistivities," *Inverse Problems Eng.*, 2001a (in press).

Heikkinen, L. M., Vauhkonen, M., Savolainen, T. and Kaipio, J. P., "Modelling of Internal Structures and Electrodes in Electrical Process Tomography," *Measurement Science and Technology*, **12**, 2001b (in press).

Hua, P., Webster, J. G. and Tompkins, W. J., "A Regularised Electrical Resistance Tomography Reconstruction Algorithm," *Clin. Phys. Physiol. Meas.*, **9**, **Sup. A**, 137 (1988).

Jones, O. C., Lin, J. T., Ovacik, L. and Shu, H., "Impedance Imaging Relative to Gas-Liquid Systems," *Nucl. Eng. Des.*, **141**, 159 (1993).

Kim, M. C., Kim, S., Kim, K. Y. and Lee, Y. J., "Regularization Methods in Electrical Impedance Tomography Technique for the Two-Phase Flow Visualization," *Int. Comm. Heat and Mass Transfer*, **28**, 773 (2001).

Lyon, G. M. and Oakley, J. P., "A Simulation Study of Sensitivity in Stirred Vessel Electrical Impedance Tomography," Tomography Techniques for Process Design and Operation, Computational Mechanics Publications, Southampton, UK, pp. 137-146 (1993).

Ovacik, L. and Jones, O. C., "Development of an Electrical Impedance Computed Tomographic Two-phase Flows Analyzer," USDOE Report, DE-FG07-90ER13032 (1998).

Vauhkonen, M., "Electrical Impedance Tomography and Prior Information," PhD. Thesis, University Kuopio, Finland (1997).

Webster, J. G., "Electrical Impedance Tomography," Adam Hilger (1990).

Williams, R. A., Jia, X. and McKee, S. L., "Development of Slurry Mixing Models Using Resistance Tomography," *Powder Technology*, **87**, 21 (1996).

Yorkey, T. J., Webster, J. G. and Tompkins, W. J., "Comparing Reconstruction Algorithms for Electrical Resistance Tomography," *IEEE Trans. Biomed. Eng.*, **34**, 843 (1987).